Topological derivative-based multi-material structural optimization with adaptive mesh refinement

Jorge Morvan Marotte Luz Filho[1], Antonio André Novotny[1]

[1]*Coordenação de Métodos Matemáticos e Computacionais, Laboratório Nacional de Computação Científica LNCC/MCTI*
Av. Getúlio Vargas 333, 25651-075 Petrópolis - RJ, Brasil
jmorvan@lncc.com.br, novotny@lncc.com.br

Abstract. Topology optimization of structures has been a topic great interest and intense research in the last decades. In simple terms, topology optimization aims at finding a material distribution within a given design domain which minimizes a shape functional. Typically, most works in this area mainly focus on considering the problem of obtaining optimal topologies composed of a single material. However, recent efforts and developments allowed for the incorporation of more than one material in the optimization problem. More specifically, we adopt here a topology optimization algorithm based on the topological derivative together with a domain representation on a fixed mesh with the help of multiple level-set functions. The topological derivative measures the sensitivity of a given shape functional with respect to an infinitesimal singular domain perturbation, such as holes, inclusions, source terms or cracks. In this work, the topological derivative is used in the optimization procedure as a steepest descent direction, like in any method based on the gradient of the cost functional. In addition, adaptive mesh refinement procedures are performed as a part of the optimization scheme for an enhanced boundary resolution of the final topology. Finally, numerical experiments of classical benchmarks in structural optimization are performed into two and three spaces dimensions to show the effectiveness of the proposed approach.

Keywords: Topological derivative method, multi-material, topology optimization

1 Introduction

Structural optimization has been a topic of great interest for over 100 years. The recent developments in this area, specially in the past two decades, have qualified it as important tool in the design process. In simple terms, it allows the designer to obtain optimized structures with reduced human intervention. One interesting aspect regarding the recent and increasing developments in multi-material topology optimization, is the fact that the resulting optimal topologies can be perfectly constructed with additive manufacturing techniques. Therefore, the development of new design strategies, such as level-set based approaches for instance, is crucial to keep pace with the technological advances. The level set method was first introduced by [1] for moving interface problems. Its main feature lies precisely in the ability to track and smoothly represent the evolution of interface boundaries on a fixed mesh, which ultimately leads to fast numerical algorithms [2]. Thus, level-set techniques have been successfully applied for solving topology optimization problems as an alternative approach to the traditional density-based methods. In order to deal with the multi-material topology optimization problem, several variations of the level-set method have been proposed, with two approaches standing out form the others [3]. The first one, called Color level-set, was proposed by Wang & Wang [4] and it uses n level-set functions to represent 2^n material regions. The main issue of this approach is the interpretation of redundant material regions that appear whenever the number of material regions to be represented is not exactly 2^n, making the analysis much more involved. An application of this strategy in the context of multi-phase structural optimization can be found [5]. The second approach, called Multi-Material Level-Set Method (MM-LS), was proposed by Wang et al. in [6] and it consists in representing $n+1$ material plus void regions by employing a combinatorial scheme of n level-set functions. It is important to emphasize that this approach ensures no overlapping regions and naturally avoids the problem of redundant regions in the project domain. The recent work by Romero & Giusti [3] uses the MM-LS scheme together with the topological

derivative method in the context of multi-material topology optimization in many different applications.

In the present work, we adapt the topology optimization algorithm based on the topological derivative method together with a LL-MS proposed in [3] to use adaptive instead of structured mesh refinement and also extend it to three spatial dimensions. The work is organized as follows: In Section 2 a brief explanation of the MM-LS is provided. The problem formulation is stated in Section 3. The topological derivative method is introduced in Section 4 and in Section 5 the topology optimization algorithm is explained. Finally, two numerical results showing the effectiveness of the proposed approach are presented in Section 6.

2 Multi-material level-set representation

Consider a geometrical domain $\Omega \subset \mathbb{R}^d$, with $d = 2, 3$ which can be decomposed into $n + 1$ regions such that

$$\Omega = \bigcup_{i=0}^{n} \Omega_i \quad \text{and} \quad \Omega_i \cap \Omega_j = \emptyset \quad \forall i \neq j \ , \tag{1}$$

where Ω_i is the geometrical domain assigned to the i-th material. The region Ω_0 represents the void region whereas the last n regions are assigned to solid materials. Now, let $\boldsymbol{\Psi}(x) = [\Psi_1(x), \Psi_2(x), \ldots, \Psi_n(x)]^\top$ be a vector of n level-set functions. Then, let us define the heaviside vector $\boldsymbol{H}(\boldsymbol{\Psi}) = [H(\Psi_1), H(\Psi_2), \ldots, H(\Psi_n)]^\top$, with its components given by

$$H(\Psi_i(x)) = \begin{cases} 1, & \text{if } \Psi_i(x) \leq 0 \\ 0, & \text{if } \Psi_i(x) > 0 \ . \end{cases} \tag{2}$$

From the above definitions, the MM-LS approach proposed by Wang [6] establishes a vector of characteristic functions $\boldsymbol{\chi} = [\chi_n^0, \chi_n^1, \ldots, \chi_n^n]^\top$ built in combinatory fashion, namely:

$$\begin{aligned} \chi_n^0 &= (1 - H(\Psi_1)) \ , \\ \chi_n^1 &= (1 - H(\Psi_2)) \prod_{i=1}^{1} H(\Psi_i) \ , \\ \chi_n^2 &= (1 - H(\Psi_3)) \prod_{i=1}^{2} H(\Psi_i) \ , \\ &\vdots \\ \chi_n^k &= (1 - H(\Psi_{k+1})) \prod_{i=1}^{k} H(\Psi_i) \ , \\ &\vdots \\ \chi_n^{n-1} &= (1 - H(\Psi_n)) \prod_{i=1}^{n-1} H(\Psi_i) \ . \end{aligned} \tag{3}$$

Note that, each component of the vector $\boldsymbol{\chi}$ indicates the presence of a specific material at the point $x \in \Omega$. Thus, the material regions are represented as

$$\chi_n^i(x) = \begin{cases} 1, & \text{if } x \in \Omega_i \\ 0, & \text{if } x \notin \Omega_i \ . \end{cases} \tag{4}$$

In addition, only n level set functions are necessary to represent the n material regions plus the void region. For a more detailed description of the MM-LS approach, see [6].

3 Problem formulation

Let us consider an open and bounded domain $\Omega \subset \mathbb{R}^d$, with Lipschitz boundary denoted as $\Gamma := \partial\Omega$. The boundary Γ is the union of two given non-overlapping subsets Γ_D and Γ_N, that is $\partial\Gamma = \Gamma_D \cup \Gamma_N$ and

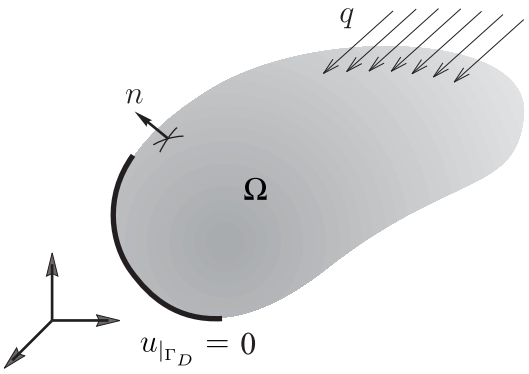

Figure 1. The elasticity problem.

$\Gamma_D \cap \Gamma_N = \varnothing$. On Γ_D the displacements are prescribed, whereas the boundary tractions are prescribed on Γ_N. See Figure 1.

In this work, we are interested in solving the classical compliance topology optimization problem of structures subject to an external load under volume constraint as stated in Section 5 in the book by [7]. Such a problem, in our context, consists in finding the $n+1$ material regions $\Omega_i \subset \Omega$, $i = 0, 1, \ldots, n$, that solve the following minimization problem:

$$\underset{\Omega_0,\Omega_1,\ldots,\Omega_n \subset \Omega}{\text{Minimize}} \mathcal{F}(u) := \mathcal{C}(u) + \sum_{i=0}^{n} \beta_i |\Omega_i| \ . \tag{5}$$

where $\beta_i > 0$ is a fixed multiplier used to impose a volume constraint for the i-th material region of the form $|\Omega_i| \leq M_i$, with $M_i > 0$, and $\mathcal{C}(u)$ is the structural compliance, namely

$$\mathcal{C}(u) = \int_{\Gamma_N} q \cdot u \ , \tag{6}$$

with q the prescribed traction on Γ_N and u the solution to:

$$\int_{\Omega} \sigma(u) \cdot (\nabla \eta)^s = \int_{\Gamma_N} q \cdot \eta \ , \quad \forall \eta \in \mathcal{V} \ , \tag{7}$$

where $\mathcal{V} = \mathcal{U} := \{\varphi \in H^1(\mathcal{D}; \mathbb{R}^d) : \varphi_{|\Gamma_D} = 0\}$. The Cauchy stress tensor $\sigma(u)$ is given by

$$\sigma(u) = \mathbb{C}(\boldsymbol{\chi})(\nabla u)^s \ , \tag{8}$$

with the constitutive tensor

$$\mathbb{C}(\boldsymbol{\chi}) = \sum_{i=0}^{n} \chi_n^i \mathbb{C}_i; \ , \tag{9}$$

where $\mathbb{C}_i$ is the fourth order constitutive tensor of the i-th material. For an isotropic and homogeneous material, it may be written as follows

$$\mathbb{C}_i = 2\mu_i \mathbb{I} + \lambda_i (\mathrm{I} \otimes \mathrm{I}) \ , \tag{10}$$

where I and $\mathbb{I}$ are the second- and fourth-order identity tensors, respectively, μ_i and λ_i are the Lamé's coefficients of the i-th material. In particular, in the case of plane stress assumptions, we have the following coefficients

$$\mu_i = \frac{E_i}{2(1+\nu_i)} \quad \text{and} \quad \lambda_i = \frac{\nu_i E_i}{1-\nu_i^2} \ , \tag{11}$$

whereas in the case of plane strain state, they are

$$\mu_i = \frac{E_i}{2(1+\nu_i)} \quad \text{and} \quad \lambda = \frac{\nu_i E_i}{(1+\nu_i)(1-2\nu_i)} \ , \tag{12}$$

where E_i and ν_i are, respectively, the Young's modulus the Poisson's ratio of the $i-th$ material. Finally, the strain tensor is given by

$$(\nabla u)^s = \frac{1}{2} \left(\nabla u + (\nabla u)^\top \right) \ , \tag{13}$$

4 The topological derivative method

The topological derivative is defined as the first term of the asymptotic expansion of a given shape functional with respect to a small parameter that measures the size of singular domain perturbations, such as holes, inclusions, source-terms and cracks. In other words, the topological derivative measures the sensitivity of the associated shape functional with respect to the nucleation of a singular domain perturbation. This concept can naturally be used as a steepest-descent direction in an optimization process like in any method based on the gradient of the cost functional. Thus, this relatively new concept has applications in many different fields such as shape and topology optimization, inverse problems, imaging processing, multi-scale material design, and mechanical modeling including damage and fracture evolution phenomena [7].

4.1 The topological derivative concept and topological gradients

Let us consider an open and bounded domain $\Omega \subset \mathbb{R}^d$, which is subject to a non-smooth perturbation confined in a small region $B_\varepsilon(\hat{x})$ of size ε, where $\hat{x}$ is an arbitrary point of Ω. Then, by introducing the characteristic function χ associated with the unperturbed domain, we may also define a characteristic function associated with the topologically perturbed domain χ_ε. In the case of a perforation, for example, $\chi_\varepsilon(\hat{x}) = \chi - (1-\gamma)\chi_{\overline{B}_\varepsilon(\hat{x})}$, where $\gamma \in \mathbb{R}^+$ is the constrast parameter in the material property. Next, we assume that a given functional $\mathcal{F}(\chi_\varepsilon(\hat{x}))$, associated with the topologically perturbed domain, admits a topological asymptotic expansion of the form

$$\mathcal{F}(u_\varepsilon, \chi_\varepsilon(\hat{x})) = \mathcal{F}(u, \chi) + f(\varepsilon) D_T(\mathcal{F}(u, \chi), \hat{x}) + o(f(\varepsilon)) \,, \tag{14}$$

where $\mathcal{F}(u, \chi)$ is the functional associated with the unperturbed domain, $f(\varepsilon)$ is a positive function such that $f(\varepsilon) \to 0$ when $\varepsilon \to 0$, and $o(f(\varepsilon))$ is the remainder term, that is, $o(f(\varepsilon))/f(\varepsilon) \to 0$ when $\varepsilon \to 0$. The function $\hat{x} \mapsto D_T(\mathcal{F}(u, \chi), \hat{x})$ is called the *topological derivative* of $\mathcal{F}(u, \chi)$ at $\hat{x}$. Therefore, the product $f(\varepsilon) D_T(\mathcal{F}(u, \chi), \hat{x})$ represents a first order correction over $\mathcal{F}(u, \chi)$ to approximate $\mathcal{F}(u_\varepsilon, \chi_\varepsilon(\hat{x}))$. In addition, after rearranging (14), we have

$$\frac{\mathcal{F}(u_\varepsilon, \chi_\varepsilon(\hat{x})) - \mathcal{F}(u, \chi)}{f(\varepsilon)} = D_T\mathcal{F} + \frac{o(f(\varepsilon))}{f(\varepsilon)} \,, \tag{15}$$

where we have replaced $D_T(\mathcal{F}(u, \chi), \hat{x})$ by $D_T\mathcal{F}$ for the sake of simplicity. The limit passage $\varepsilon \to 0$ in the above expression leads to the general definition for the *topological derivative*, namely

$$D_T(\hat{x}) := \lim_{\varepsilon \to 0} \frac{\mathcal{F}(u_\varepsilon, \chi_\varepsilon(\hat{x})) - \mathcal{F}(u, \chi)}{f(\varepsilon)} \,. \tag{16}$$

Note that, by considering only one material and void, there exists a sensitivity to a topological perturbation due to an introduction of a hole in the material region and another one due to the introduction of a reinforcement in the void region. Therefore, in this case the topological derivative is defined by pairs, in order to consider the two sensitivities above mentioned. Since both sensitivities are measured in the entire domain, the sensitivity due to an introduction of a hole in the void region will be zero. Analogously, the sensitivity due to a reinforcement of the same material in the material region will also be zero. In this sense, the following topological gradient $g(x)$ is defined in such a way that we have a single that measures the sensitivity of $\mathcal{F}$ with respect to an oriented shift to the topology:

$$g(x) := \begin{cases} -D_T^-\mathcal{F}, & \text{if } x \in \Omega_{mat} \\ D_T^+\mathcal{F}, & \text{if } x \in \Omega_{void} \,. \end{cases} \tag{17}$$

In addition, we may even write the topological gradient g in the form

$$g(x) = -\chi_{mat} D_T^-\mathcal{F} + (1 - \chi_{mat}) D_T^+\mathcal{F} \,, \tag{18}$$

where D_T^- and D_T^- are the topological derivatives due to the introduction of a hole in the material region and due to the introduction of a solid inclusion in the void region, respectively, and χ_{mat} is the characteristic function associated with the material region Ω_{mat}.

Now, according to the domain representation method presented in Section 2, the topological gradient can be constructed as [8]

$$g_k(x) = -\sum_{i=k}^{n} \chi_n^i D_T\mathcal{F}^{i\to(k-1)} + \chi_n^{k-1} \sum_{i=k}^{n} \frac{\partial \chi_n^i}{\partial \chi_n^k} D_T\mathcal{F}^{(k-1)\to i} \,, \tag{19}$$

where $g_k(x)$ is the k-th component of the topological gradient vector

$$\boldsymbol{g}(x) = [g_1(x), g_2(x), \ldots, g_k(x), \ldots, g_n(x)]^\top \ . \tag{20}$$

The term $D_T\mathcal{F}^{i\to j}$ represents the sensitivity of the functional due to the introduction of a singular perturbation made of material j on the base material i at the point $\hat{x}$. The topological derivative of the shape functional defined in (5) is

$$D_T^{i\to j}\mathcal{F}(x) = D_T^{i\to j}C(x) + \beta_i D_T^{i\to j}|\Omega|. \tag{21}$$

with the topological derivative of the compliance shape functional given by

$$D_T^{i\to j}\mathcal{C}(x) = -\mathbb{P}_\gamma^{i\to j}\sigma(u(x)) \cdot \nabla(u)^s \ , \tag{22}$$

where the polarization tensor $\mathbb{P}_\gamma$, for $\nu_0 = \nu_1 = \cdots = \nu_n$, is given by the following fourth-order isotropic tensor

$$\mathbb{P}_\gamma^{i\to k} = -\frac{1-\gamma^{i\to k}}{1+\gamma^{i\to k}\alpha_2}\left((1+\alpha_2)\mathbb{I} + \frac{1}{2}(\alpha_1-\alpha_2)\frac{1-\gamma^{i\to k}}{1+\gamma^{i\to k}\alpha_2}(\mathrm{I}\otimes\mathrm{I})\right) \quad \text{for} \quad d=2 \ , \tag{23}$$

with

$$\alpha_1 = \frac{\lambda_i+\mu_i}{\mu_i} \quad \text{and} \quad \alpha_2 = \frac{\lambda_i+3\mu_i}{\lambda_i+\mu_i} \ . \tag{24}$$

$$\mathbb{P}_\gamma^{i\to k} = -(1-\gamma^{i\to k})[3\alpha_2\mathbb{I} + (\alpha_1-\alpha_2)\mathrm{I}\otimes\mathrm{I}] \quad \text{for} \quad d=3 \ , \tag{25}$$

with with the constants α_1 and α_2 given by

$$\alpha_1 = \frac{1-\nu_i}{3(1-\nu_i)-(1+\nu_i)(1-\gamma^{i\to k})} \quad \text{and} \quad \alpha_2 = \frac{5(1-\nu_i)}{15(1-\nu_i)-(8-10\nu_i)(1-\gamma^{i\to k})} \ . \tag{26}$$

Finally, the topological derivative associated with the volume constraint is trivially obtained and given by

$$D_T^{i\to j}|\Omega_i|(x) = \begin{cases} -1, & \text{if } x \in \Omega_i \ , \\ +1, & \text{if } x \notin \Omega_i \ , \end{cases} \tag{27}$$

More details about the derivation of this result can be found in [9, 10].

5 Topology optimization algorithm

The main idea of the topology optimization algorithm used in the present work basically lies in achieving a local optimality condition for the minimization problem (5), given in terms of the topological derivative and the MM-LS introduced in the earlier sections of this work. Whenever the topological gradient $\boldsymbol{g}$ becomes parallel to the vector level-set $\boldsymbol{\Psi}$ in a $L^2(\Omega)$ sense configures a first order optimality criterion for the topology optimization problem, which can be stated as [2, 3]

$$\theta := \arccos\left[\frac{\langle \boldsymbol{g}, \boldsymbol{\Psi}\rangle_{L^2(\mathcal{D})}}{\|\boldsymbol{g}\|_{L^2(\mathcal{D})}\|\boldsymbol{\Psi}\|_{L^2(\mathcal{D})}}\right] = 0 \ , \tag{28}$$

Now, with all the elements introduced so far, we may provide a brief explanation of the algorithm is. We start by choosing an initial level-set vector function $\boldsymbol{\Psi}_0$. In a generic iteration m, we compute the function $\boldsymbol{g}_m$ associated with the level-set function $\boldsymbol{\Psi}_m$. Then, the new level-set function $\boldsymbol{\Psi}_{m+1}$ is updated according to the following linear combination of the functions $\boldsymbol{g}_m$ and $\boldsymbol{\Psi}_m$

$$\boldsymbol{\Psi}_{m+1} = \frac{1}{\sin\theta_m}\left[\sin((1-w)\theta_m)\boldsymbol{\Psi}_m + \sin(w\theta_m)\frac{\boldsymbol{g}_m}{\|\boldsymbol{g}_m\|_{L^2(\mathcal{D})}}\right] \text{ with } k = 1, 2, \ldots, n \ . \tag{29}$$

where θ_m is the angle between $\boldsymbol{g}_m$ and $\boldsymbol{\Psi}_m$, and w is a step size determined by a linear search performed in order to decrease the value of the objective function $\mathcal{F}$ associated with $\boldsymbol{\Psi}_m$. The step size w is initially chosen as 1 and decreases accordingly to $w \leftarrow w/2$ until the condition $\mathcal{F}_{m+1} < \mathcal{F}_m$ is fulfilled. The process ends whenever the condition $\theta_m \leq \epsilon_\theta$ is satisfied at some iteration, with ϵ_θ a given small numerical tolerance. If at some iteration the line-search step size w is found to be smaller than a given numerical tolerance $\epsilon_w > 0$ and the local optimality condition is not satisfied, then an adaptive mesh refinement is performed and the iterative process is continued. In all numerical experiments, we consider $\epsilon_\theta = 1^\circ$ and $\epsilon_w = 1.0 \times 10^{-3}$.

6 Numerical results

In this section, we present one classical example in structural optimization of a cantilever beam in two space dimensions to be optimized with two material regions. In addition, we propose a benchmark example in three spatial dimensions also to be optimized considering two material regions. In both examples, the following material properties were considered: $E_1 = 1$, $E_2 = E_1/2$, $E_0 = E_1 \times 10^{-3}$ and $\nu_0 = \nu_1 = \nu_2 = 1/3$. The subscripts $1, 2$ refer to the material region whereas the subscript 0 refers to the void region. In addition, the material regions 1 and 2 are, respectively, represented by red and blue colors.

6.1 2D example

We consider here the classical example of a cantilever beam of dimension $2 \times 1\ m^2$ under plane stress state and subject to a loading force $q = (0.0, -1.0)$ at the center of the right side. The final topology was obtained after 43 iterations and one adaptive mesh refinement with the optimality condition fulfilled, namely $\theta_{43} = 0.94$. In addition, a final volume fraction $|\Omega_1| \approx 20\%$ and $|\Omega_2| \approx 35\%$ for the material regions was obtained for the optimal topology. The project domain and boundary conditions, as well as the final topology are shown in Figure 2.

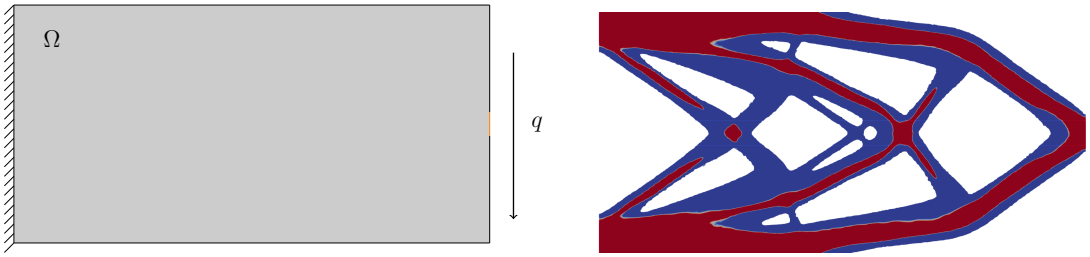

Figure 2. Example 1: Initial domain and boundary conditions and final result.

6.2 3D example

Now, let us consider a cube of dimensions $5 \times 5 \times 5\ m^3$ with hinge supports at the bottom. The cube is also subject to a surface traction $q = (0.0, 0.0, -1.0)$ distributed in a small square region of dimensions $0.5 \times 0.5\ m^2$ at the center of the top face. The hinge supports are also squares of dimension $0.25 \times 0.25\ m^2$ with their centers at $0.375\ m$ from the edges of the cube, as shown in Figure 3. The final topology was obtained after 70 iterations and

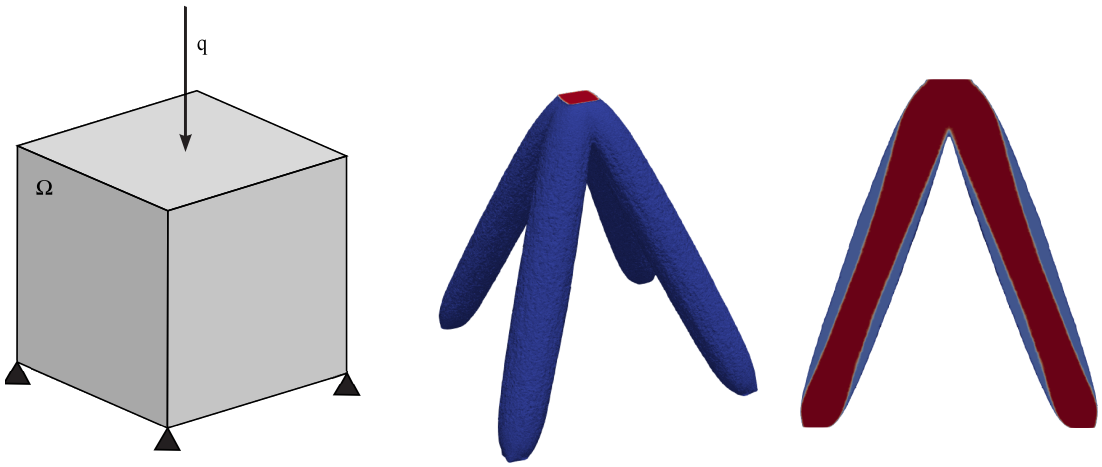

Figure 3. Example 2: Initial domain and boundary conditions, perspective and diagonal cut views of the final topology.

three adaptive mesh refinements. The optimality condition was fulfilled at the end of the iterative process, namely $\theta_{70} = 0.88°$. A final volume fraction $|\Omega_1| \approx 4.5\%$ and $|\Omega_2| \approx 4.0\%$ for the material regions was obtained for the optimal topology. A perspective view, as well as diagonal cut of the optimal topologies are shown in Figure 3.

7 Conclusions

This work deals with structural optimization using the topological derivative method and MM-LS for the representation of the material regions. The main contributions of this work is the use of adaptive mesh refinement and extending an existing topologcial derivative-based approach to the three-dimensional scenario. The use of adaptive mesh refinement in the process has proved to be very effective in enhancing the boundary representation of the material regions in the final topology.

Acknowledgements. the authors would like to acknowledge the funding received by CNPq (Brazilian Research Council), CAPES (Brazilian Higher Education Staff Training Agency) and FAPERJ (Research Foundation of the State of Rio de Janeiro).

Authorship statement. The authors hereby confirm that they are the sole liable persons responsible for the authorship of this work, and that all material that has been herein included as part of the present paper is either the property (and authorship) of the authors, or has the permission of the owners to be included here.

References

[1] S. Osher and J. A. Sethian. Front propagating with curvature dependent speed: algorithms based on Hamilton-Jacobi formulations. *Journal of Computational Physics*, vol. 79, n. 1, pp. 12–49, 1988.
[2] S. Amstutz and H. Andrä. A new algorithm for topology optimization using a level-set method. *Journal of Computational Physics*, vol. 216, n. 2, pp. 573–588, 2006.
[3] A. A. Romero and S. M. Giusti. A robust topological derivative-based multi-material optimization approach: Optimality condition and computational algorithm. *Computer Methods in Applied Mechanics and Engineering*, vol. 366, n. 113044, 2020.
[4] M. Y. Wang and X. Wang. ''color'' level sets: a multi-phase method for structural topology optimization with multiple materials. *Computer Methods in Applied Mechanics and Engineering*, vol. 193, n. 6–8, pp. 469–496, 2004.
[5] G. Allaire, C. Dapogny, G. Delgado, and G. Michailidis. Multi-pase structural optimization via a level set method. *ESAIM: Control, Optimisation and Calculus of Variations*, vol. 20, pp. 576–611, 2014.
[6] Y. Wang, Z. Luo, and Z. Kang. A multi-material level set-based topology and shape optimization method. *Computer Methods in Applied Mechanics and Engineering*, vol. 283, n. 1, pp. 1570–1586, 2015.
[7] A. Novotny and J. Sokołowski. *An introduction to the topological derivative method*. Springer Briefs in Mathematics. Springer Nature Switzerland, 2020.
[8] N. Kishimoto, Y. Noguchi, Y. Sato, K. Izui, and T. Yamada. Topology optmization for multi-material structures based on the level-set method. *Trans JSME*, vol. 83, n. 849, pp. 17–69, 2017.
[9] S. M. Giusti, A. Ferrer, and J. Oliver. Topological sensitivity analysis in heterogeneous anisotropic elasticity problem. Theoretical and computational aspects. *Computer Methods in Applied Mechanics and Engineering*, vol. 311, pp. 134–150, 2016.
[10] M. Bonnet and G. Delgado. The topological derivative in anisotropic elasticity. *The Quarterly Journal of Mechanics and Applied Mathematics*, vol. 66, n. 4, pp. 557–586, 2013.